Inorg. Chem. **2002**, *41*, 4127−4130

Synthesis of the New Metastable Skutterudite Compound $NiSb_3$ from Modulated Elemental Reactants

Joshua R. Williams and David C. Johnson*

Department of Chemistry and Materials Science Institute, University of Oregon, Eugene, Oregon 97403

Received November 1, 2001

A new metastable binary compound with the skutterudite crystal structure has been synthesized from modulated elemental reactants, through an amorphous intermediate, using a novel low-temperature synthesis technique. The amorphous reaction intermediate undergoes nucleation at 87 °C, an extremely low temperature for solid-state reactions. When heated above 350 °C, the metastable phase $NiSb_3$ disproportionates into the thermodynamically stable phases $NiSb_2$ and Sb. Also, if the sum of the individual elemental layer thicknesses is greater than 30 Å, a mixture of different phases forms. Simulation of the high-angle powder X-ray diffraction spectrum confirms that $NiSb_3$ is isostructural with $CoSb_3$.

Introduction

Due to the extremely slow diffusion rates typical of solid-state reactions, long annealing times and high temperatures are generally required to drive reactions to completion. These synthesis conditions, however, are not conducive to the formation of compounds that are only metastable, or kinetically stable, particularly if they are thermodynamically unstable with respect to disproportionation. Unfortunately there are not many alternative solid-state synthesis methods available to prepare compounds that will only be accessible at low temperature.[1] Indeed, even the preparation of thermodynamically stable compounds that incongruently melt at low temperatures requires knowledge of the phase diagram for successful synthesis.[2]

In the past few years, we have developed a novel synthesis method that allows the synthesis of solid-state inorganic materials at low temperatures, usually lower than 500 °C. This method, called the modulated elemental reactant method, involves using a high-vacuum physical vapor deposition system to sequentially deposit ultrathin elemental layers onto a substrate. The thickness of these elemental layers, usually on the order of angstroms, determines the important diffusion distances in the subsequent interdiffusion of these layers. Since these diffusion distances are many orders of magnitude smaller than found in bulk reactions, the stacked elemental layers can be annealed at low temperature (usually below 200 °C) to complete diffusion of the elemental layers. For most systems, an initial annealing temperature can be chosen which will allow complete diffusion of the elemental layers without providing enough energy to overcome the activation energy barrier for nucleation. This produces an amorphous intermediate that, on further annealing, will undergo nucleation of a crystalline phase. Due to the low-temperature reaction conditions, long-range diffusion processes are very slow. Therefore, the composition of the amorphous phase determines which phase will nucleate, and the compound that is easiest to nucleate at the given composition will undergo nucleation, whether it is the most thermodynamically stable phase or not. In this way, we are able to "trap" kinetically stable phases.[3]

The ability to prepare new metastable compounds raises the question of how to predict the existence of new metastable phases. There are two main directions that one could take. The first would be to search for compounds with new and novel structures.[4] A second approach is to start with known compounds and structure types, and to search for variations of those structures that could potentially be synthesized. In this paper we used this second strategy. An examination of the cobalt−antimony phase diagram, as shown in Figure 1, reveals the existence of the phase $CoSb_3$,

* Author to whom correspondence should be addressed. E-mail: davej@oregon.uoregon.edu.

(1) Stein, A.; Keller, S. W.; Mallouk, T. E. *Science* **1993**, *259*, 1558−1564.
(2) Corbett, J. D. In *Synthesis of solid-state materials*; Corbett, J. D., Ed.; Clarendon Press: Oxford, 1987; pp 1−38.
(3) Johnson, D. C. *Curr. Opin. Solid State Mater. Sci.* **1998**, *3*, 159−167.
(4) Schon, J. C.; Jansen, M. *Angew. Chem.* **1996**, *35*, 1286−1304.

10.1021/ic011131j CCC: $22.00
Published on Web 07/17/2002

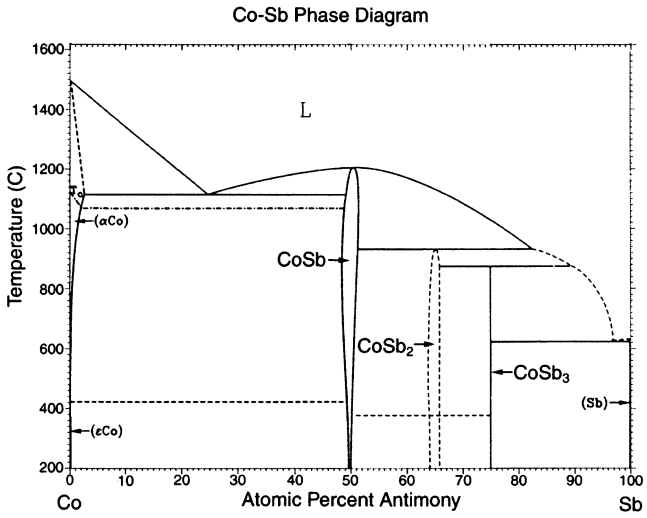

Figure 1. The Co−Sb phase diagram.[8]

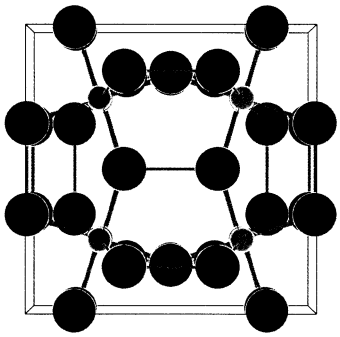

Figure 2. The skutterudite crystal structure where the small-diameter balls indicate the positions of cobalt atoms and the larger diameter circles represent the positions of antimony atoms. Projection is along the (100) axis.

which has the skutterudite structure type shown in Figure 2. This structure type is currently of great interest to the thermoelectric community due to the demonstrated potential of "filling" the void in the structure with small heavy atoms, resulting in a reduction of the thermal conductivity of the material.[5,6] Upon comparing the nickel−antimony phase diagram shown in Figure 3 with the cobalt−antimony phase diagram in Figure 1, one observes that they are very similar above 40% antimony. They both contain 1:1 and 1:2 compounds with identical structures stable in similar composition ranges. The main difference in this region is the existence of the incongruently melting $CoSb_3$ and the absence of an isostructural compound in the Ni−Sb phase diagram. Considering the similarities in these phase diagrams, we decided to search for the existence of an analogous metastable skutterudite phase. With this goal in mind, several modulated elemental reactants were synthesized, varying the relative layer thickness of nickel and antimony to adjust the overall composition of the sample as well as the repeat layer thickness (the sum of both elemental layer thicknesses).

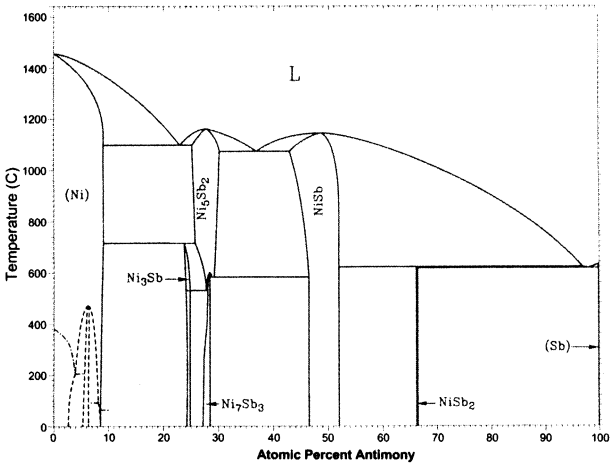

Figure 3. The Ni−Sb phase diagram.[8]

Experimental Section

Layer deposition was performed in a custom-built high-vacuum deposition chamber with multiple sources and targets, which is described elsewhere.[7] A personal computer and custom automation software are used to control the deposition. Nickel was evaporated from a Thermionics electron-beam gun at a rate of ~0.5 Å/s. Antimony was evaporated from a custom-built Knudsen cell at a rate of ~0.8 Å/s. Deposition rates and thicknesses were monitored using Leybold Inficon XTC/2 quartz crystal thickness monitors.

The films were deposited onto polished silicon wafer pieces (for low-angle X-ray diffraction), miscut quartz pieces (for high-angle X-ray diffraction), and silicon wafers coated with poly(methyl methacrylate) (PMMA). The coated wafers were then soaked in acetone to dissolve the PMMA and allow the multilayer films to lift off of the wafer surface. The pieces of film were then collected by vacuum filtration using Teflon filter papers.

Sample composition was determined using electron probe microanalysis (EPMA) using a Cameca S-50 instrument, a 10 keV accelerating voltage, a 10 nA beam current, and a 1 μm spot size. High-angle diffraction data on the powder after differential scanning calorimetry was obtained on a Scintag SDS-2000 $\theta-2\theta$ diffractometer using a piece of miscut quartz as the sample holder. High-angle diffraction data on the film-coated miscut quartz pieces, as well as all low-angle diffraction data, was obtained using a Philips X'Pert five-circle diffractometer. All X-ray experiments were performed using Cu Kα radiation. A TA Instruments DSC 2920 modulated DSC was used to collect all DSC data. The heat flow in and out of the sample is monitored as the sample temperature is elevated at a specific rate to determine at what temperature phase changes and nucleation events occur. Approximately 0.500 mg of sample is placed and sealed inside an Al sample pan. The samples were heated under flowing nitrogen at a rate of 2 °C/min up to either 200 or 250 °C.

Results

A list of the samples prepared in this study is shown in Table 1. The intended repeat thickness for each sample (the sum of the individual elemental layer thicknesses) is shown

(5) Sales, B. C.; Mandrus, D.; Williams, R. K. *Science* **1996**, *272*, 1325−1328.
(6) Nolas, G. S.; Slack, G. A.; Morelli, D. T.; Tritt, T. M.; Ehrlich, A. C. *J. Appl. Phys.* **1996**, *79*, 4002−4008.
(7) Fister, L.; Li, X. M.; Novet, T.; McConnell, J.; Johnson, D. C. *J. Vac. Sci. Technol., A* **1993**, *11*, 3014−3019.
(8) Massalski, T. B.; Okamoto, H.; Subramanian, P. R.; Kacprzak, L. In *Binary Alloy Phase Diagrams*, 2nd ed.; Massalski, T. B., Okamoto, H., Subramanian, P. R., Kacprzak, L., Eds.; ASM International: Materials Park, OH, 1990; Vol. 3, pp 2664−2665.

Table 1. Summary of Samples Prepared Showing Layer Thickness (Å), Composition, and Phase Formation

sample	intended thickness (Å) Ni	intended thickness (Å) Sb	thickness % Sb	atomic % A% Ni	atomic % A% Sb	bilayer thickness (Å) intended	bilayer thickness (Å) actual	phase(s) formed
1	0.5	15	0.97	17.3	82.3	15.5	15.1	$NiSb_3$
2	0.75	15	0.95	24.8	75.2	15.8	15.6	$NiSb_3$
3	1	15	0.94	32.2	67.7	16	15.0	$NiSb_2$, Sb
4	1.25	15	0.92	34.3	65.7	16.25	15.2	$NiSb_2$, Sb
5	0.4	15	0.97	15.1	84.9	15.4	14.6	$NiSb_3$
6	1.5	30	0.95	30.2	69.7	31.5	28.0	$NiSb_2$, Sb
7	0.75	15	0.95	25.6	74.4	15.8	15.2	$NiSb_3$
8	0.8	30	0.97	22.6	77.4	30.8	30.2	$NiSb_3$, Sb
9	1.6	60	0.97	17.9	82.1	61.6	56.9	$NiSb_3$, Sb
10	2	75	0.97	17.1	82.9	77	62.9	$NiSb_2$, Sb
11	0.4	15	0.97	24.9	75.1	15.4	14.7	$NiSb_3$
12	0.5	15	0.97	27.7	72.3	15.5	15.5	$NiSb_2$, Sb
13	0.35	15	0.98	20.3	79.7	15.4	13.8	$NiSb_3$
14	0.4	15	0.97	18	82	15.4	13.9	$NiSb_3$
15	0.35	15	0.98	20.3	79.6	15.4	14.0	$NiSb_3$

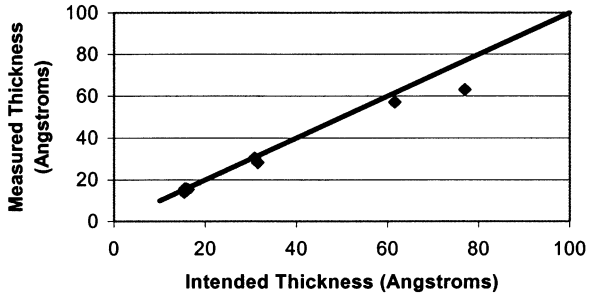

Figure 4. A graph of the intended bilayer thickness and the observed bilayer thickness determined using low-angle X-ray diffraction. The line drawn is the expected linear relationship between these thicknesses.

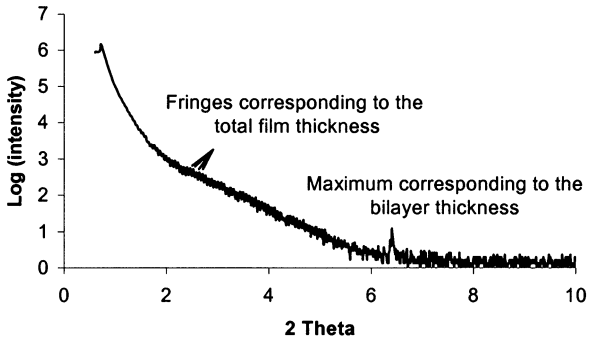

Figure 5. Low-angle X-ray diffraction spectrum illustrating both a Bragg diffraction maximum resulting from the repeat thickness and the front/back film reflections.

as well as the intended thickness of each elemental layer. Figure 4 shows the agreement of the intended thickness (determined from the deposition parameters) to the measured layer thicknesses determined directly from low-angle X-ray diffraction data. Layer thickness is determined using Bragg diffraction maxima in the low-angle X-ray diffraction, a sample of which is shown in Figure 5, or by finding the total film thickness from the front/back reflections in the low-angle X-ray diffraction spectra, and dividing by the number of repeats deposited. In some cases neither front/back reflections nor Bragg peaks were observed presumably as a result of sample roughness. While the agreement between the intended thickness and the actual thickness of the layers in the samples is within an angstrom, the small changes in intended nickel layer thickness are less than the standard deviation in Figure 4. In Figure 6 we graph the percent

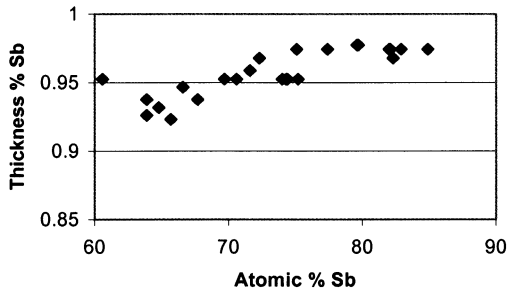

Figure 6. Intended composition (from intended layer thicknesses) vs measured composition determined using microprobe analysis.

antimony thickness (i.e., thickness of Sb/thickness of Sb + thickness of Ni) versus atomic percent antimony determined from microprobe analysis. In general there is good agreement between the intended and measured composition. The largest source of error results from small positional changes of the deposition sources as they are reinstalled over the time required for this study.

We began this study by preparing several samples, with compositions both antimony rich and antimony poor relative to the ideal 1:3 Ni:Sb ratio of our proposed compound, to determine the effect of composition on phase formation. To minimize interference from interdiffusion effects, this initial set of samples was prepared with repeat layer thickness below 20 Å. The absence of Bragg diffraction maxima in the low-angle diffraction spectra for most of these samples suggests that either some diffusion has occurred on deposition or the layering is very nonuniform. We observed that the phase formed depends very strongly on the overall composition of the sample. If the Sb:Ni ratio is even slightly below 3:1, the thermodynamically stable phase $NiSb_2$ forms, as well as Sb. If the composition is more Sb rich, $NiSb_3$ forms. We observed no instances of samples composed of thin repeating bilayers where the phase formation deviated from this composition dependence. This strong dependence on the overall sample composition suggests that the samples do in fact become homogeneous before nucleation occurs.

The formation of both $NiSb_2$ and $NiSb_3$ is clearly visible in a DSC trace of the as deposited samples. On heating samples with an Sb:Ni ratio below 3:1, a sharp exotherm is observed at 92 °C. Diffraction scans before this exotherm show no high-angle diffraction peaks, while after this

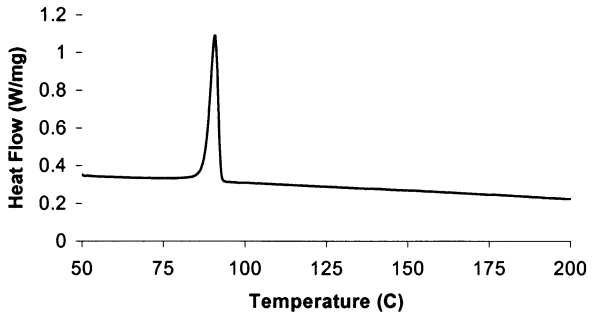

Figure 7. A differential scanning calorimetry (DSC) trace showing a clear exothermic nucleation event for the formation of $NiSb_3$.

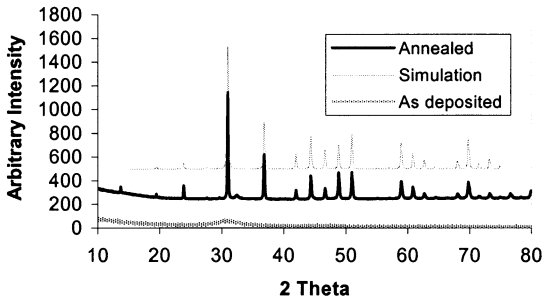

Figure 8. High-angle X-ray diffraction of a sample forming $NiSb_3$ before and after annealing. A powder diffraction simulation assuming the skutterudite structure is superimposed over the postannealing scan. Additional peaks correspond to metallic Sb.

exotherm the expected diffraction maxima from the known compound $NiSb_2$ are observed. If the ratio is at or above 3:1, however, the targeted metastable skutterudite phase $NiSb_3$ forms. A representative sample of the DSC traces observed from samples that form $NiSb_3$ is shown in Figure 7. A clear exothermic peak is observed at 87 °C. High-angle diffraction of this sample before and after the annealing in the DSC is shown in Figure 8. The diffraction data clearly demonstrates that the exothermic peak observed in the DSC trace results from the nucleation and growth of the targeted $NiSb_3$ phase. The high-angle X-ray diffraction data is modeled very well by replacing cobalt with nickel in the published structure of $CoSb_3$ and adjusting the lattice parameter to 9.13 Å, also shown in Figure 8. Rietveld refinement of the structure proved difficult due to a complex preferred orientation, which is unusual for a cubic system.

To determine the stability limits of this compound, we heated a sample in the DSC under flowing nitrogen. $NiSb_3$ appears to be only kinetically stable, as it disproportionates into the thermodynamically stable phases $NiSb_2$ and Sb upon annealing above 250 °C.

Since bulk samples do not react to form $NiSb_3$, there must exist a critical repeat layer thickness below which the samples interdiffuse without nucleating $NiSb_2$ at the reacting interface. To determine this critical thickness, samples 8−10 were prepared. These samples show a distinct change in behavior as a function of bilayer thickness. Samples with bilayer thickness below 56.9 Å and compositions antimony rich of $NiSb_3$ nucleated $NiSb_3$. Samples with layer thicknesses above 56.9 Å nucleated a mixture of different phases, including Sb with highly preferred orientation. This suggests that, in these thicker samples, nucleation is occurring at the interfaces between elemental layers before the layers can completely interdiffuse. Thus the critical bilayer thickness must lie between these two values. It should be noted that we have observed no relationship between heating rate in the DSC and critical bilayer thickness for the range of heating rates typically used in DSC experiments (1−10 °C/min).

Summary

We have demonstrated the ability to synthesize a new metastable binary skutterudite compound using the modulated elemental reactant method. The abrupt composition dependence of phase formation as well as low-angle diffraction data suggests that the sample becomes amorphous and homogeneous on initial annealing, and nucleates homogeneously upon further annealing. The new compound appears to be only kinetically stable, as it disproportionates into the thermodynamically stable phases $NiSb_2$ and Sb upon annealing above 250 °C. We have also demonstrated the importance of diffusion distance in this synthesis method by showing that the repeat layer thickness must be below 30 Å in order for the metastable phase to form.

Acknowledgment. The authors are grateful for the support of this work by ONR Contract N00014-98-1-0447 and NSF Grant DMF-9813726 at the University of Oregon.

IC011131J